厚生労働科学研究費補助金

創薬基盤推進研究事業

複数のガン防御機構を標的とした遅発型ガン発症マウスライブラリーの作製とガン予防戦略確立への応用に関する研究

平成２０年度　総括研究報告書

研究代表者　中西　真

平成２１（２００９）年　３月

目　　次

厚生労働科学研究費補助金（創薬基盤推進研究事業）
（総括）研究報告書

複数のガン防御機構を標的とした遅発型ガン発症マウスライブラリーの作製とガン予防戦略確立への応用に関する研究

研究代表者　中西　真　名古屋市立大学大学院医学研究科教授

研究要旨：ガン防御機構を制御するシステムの二重、三重変異マウスを作製し、臨床で見られる遅発型ガン発症マウスライブラリーを確立して、ガン予防戦略確立に有益であることを明らかにする。

研究分担者　なし

A. 研究目的

現在までにp53等のガン抑制遺伝子変異マウスが高率にガンを発症することが知られている。しかしながら、ヒト臨床ガンに見られるこれらガン抑制遺伝子の変異は、ガン発症の原因ではなく、むしろガン悪性化の原因か、あるいはガン進展の結果であると考えられている。実際、これらガン抑制遺伝子のノックアウトマウスは生後まもなく早期にガンを発症し、そのガンの種類もヒトの多くの臨床ガンとは大きく異なる特徴を示す。臨床ガンにおいてはチェックポイント、アポトーシス、細胞老化等の複数のガン防御機構に機能不全が蓄積することが初発原因と考えられている。これらを踏まえて、本研究ではガン防御機構を制御するシステムの二重、三重変異マウスを作製し、遅発型臨床ガン発症マウスライブラリーを確立して、ガン予防戦略確立に有益であることを明らかにする。

B. 研究方法

本研究は、研究代表者（中西真）と代表者の研究室に所属する２名の連携研究者（丹伊田浩行助教、島田緑特任助教）により、名古屋市立大学大学院医学研究科細胞生化学教室と実験動物センターを中心に行われた。平成２０年度は申請者らの研究室で開発したChk1およびChk2変異マウスを交配し、Chk1/Chk2二重変異マウスを作製して、ガン発症率およびその原因を解析した。具体的には、

1. 野生型マウス、$Chk1^{+/-}$, $Chk2^{-/-}$, $Chk1^{+/-}Chk2^{+/-}$, $Chk1^{+/-}Chk2^{-/-}$マウスにおける自然発ガン発症率を解析した。具体的には、死亡マウスを直ちに解剖し、肉眼的および組織学的解析から死因を同定した。この解析には名古屋市立大学大学院医学研究科実験病理学分野白井智之教授の協力を得て行った。

2. これら上記マウス由来のプライマリー胎児繊維芽細胞（MEFs）を用いて、DNA損傷に反応したG1/S期、およびG2/M期細胞周期停止機能を解析した。同時にDNA損傷に反応したDNA合成抑制についても明らかにした。また、DNA損傷修復能、アポトーシス誘導能についても解析した。

3. 上記MEFsを用いて、癌遺伝子誘導早期老化、高複製刺激誘導細胞老化、DNA損傷誘導早期細胞老化能を明らかにした。

（倫理面での配慮）

ノックアウトマウス作成、およびマウスの機能解析、発ガン実験に関しては、すべて名古屋市立大学医学研究科において規定された実験動物指針に基づいて行った。また適宜、厚生労働省指導の所管する実施機関における動物実験等の実施に関する基本指針を参考とし、実験動物に与える苦痛、およびストレスを必要最低限にした。

C. 研究結果

本研究の最終目標は、ヒト型遅発性ガン発症モデルマウスライブラリーを作製することにある。平成２０年度はチェックポイントに部分不全を示すChk1ヘテロマウスとアポトーシスに機能不全があるChk2ホモ欠失マウスを交配し、$Chk1^{+/-}Chk2^{-/-}$マウスを作製して、発ガン傾向およびその病態を解析した。Chk1およびChk2単独の変異マウスは野生型と比較して高発ガン性を全く示さないが、Chk1/Chk2二重変異マウスは野生型マウスに比較して、高率に遅発性のガンを発症した。ガンの組織学的解析から、多くは悪性リンパ腫であったが、肺ガン、あるいは軟部組織腫瘍等も見られ、マウス自然発ガンに見られる発ガン組織型とほぼ同じであった。具体的には、生後２０ヶ月において野生型マウスでは全くガン発症を認めなかったが、$Chk1^{+/-}Chk2^{-/-}$マウスでは７０％に、$Chk1^{+/-}Chk2^{+/-}$でも４０％にガン発症を認めた。さらに、これらマウスで見られる高発ガン性の原因を明らかにする目的で、マウス胎児繊維芽細胞

の解析を行った。Chk1ヘテロ欠失変異は、細胞周期チェックポイント異常、とりわけDNA損傷に反応したG2/M期停止の部分異常を示した。一方、Chk2の完全欠失はDNA損傷に反応したアポトーシス誘導不全をきたすことが明らかとなった。Chk2完全欠失はDNA損傷修復異常も示した。DNA損傷に反応したG1/S期停止には、Chk1およびChk2の両方が協調的に機能していることが分かった。しかしながら、発ガン防御に重要な役割を果たしているDNA損傷に反応した早期細胞老化誘導は$Chk1^{+/-}Chk2^{-/-}$マウスの胎児繊維芽細胞で維持されていた。

D. 考察

本年度の当該研究で作製した$Chk1^{+/-}Chk2^{-/-}$二重変異マウスは、早期細胞老化以外のDNA損傷反応を介した細胞応答における異常の結果、遅発型ガン発症を示した。実際、これら二重変異マウスから得られた胎児繊維芽細胞では高率に染色体異常を認めた。現在までに様々なガン抑制遺伝子が同定され、これら遺伝子のノックアウトマウスが作成されて個体レベルでの発ガンが解析されている。しかしながら、p53, INK4等の代表的なガン抑制遺伝子産物は複数のガン防御機構（細胞周期チェックポイント、アポトーシス、早期細胞老化）を制御していると考えられており、これらノックアウトマウスは非常に早期にガンを発症し、ガン予防効果の判定には不向きである。

本研究は、個々のガン防御機構を制御する因子の部分機能不全が重複することで十分個体レベルでのガン発症を誘導することを示したものであり、非常に興味深い。またこの結果は、個体レベルでのガン発症は遺伝子変異がなくてもガン防御機構に作用する因子の発現低下が重複することで誘導されることを示しており、ヒトにおけるガン発症の分子基盤の一端を解明したものと考えられる。以上のことから、$Chk1^{+/-}Chk2^{-/-}$はヒト型遅発型ガン発症モデル動物として適していると考えられる。このモデルマウスを用いて、様々な環境要因、運動、食物、化学物質等のガン発症予防効果を判定することが可能と考える。$Chk1^{+/-}Chk2^{-/-}$マウスはガン発症時期が非常に遅発的であり、またこれらマウスのガン発症原因が人に見られる突発性ガンと類似であるため、ガン予防効果の判定に非常に有用と考える。今後、別のガン防御機構の部分不全マウスを交配することで、異なる原因で遅発型にガンを発症するマウス群を作製することで、ガン予防戦略確立に有用となるヒト型ガン発症モデルマウスライブラリーを完成させていきたい。

E. 結論

$Chk1^{+/-}Chk2^{-/-}$および$Chk1^{+/-}Chk2^{+/-}$二重変異マウスは、DNA損傷に反応した一過性細胞周期停止、およびアポトーシス誘導に重複した部分不全を持つマウスであり、ヒトに見られるガン発症と同様に遅発性にガンを発症した。これらのガンはマウスで通常見られるガンと同様の組織・臓器特異性を示し、マウス個体での発ガン傾向が亢進しているものと考えられた。これらの結果は、本二重変異マウスがヒトにおけるガン予防戦略確立に有用であることを強く示唆している。

F. 健康危機情報

特にない。

G. 研究発表

1. 論文発表

Zineldeen, D.H., Shimada, M., Niida, H., Katsuno, Y., and Nakanishi, M. Ptpcd-1 is a novel cell cycle related phosphatase that regulates centriole duplication and cytokinesis. ***Biochem. Biophys. Res. Commun.*** 380, 460-466 (2009)

Nishizuka, M., Kishimoto, K., Kato, A., Ikawa, M., Okabe, M., Sato, R., Niida, H., Nakanishi, M., Osada, S., and Imagawa, M. Disruption of the novel gene fad14 causes rapid postnatal death and attenuation of cell proliferation, adhesion, spreading and migration. ***Exp. Cell Res.*** 315, 809-819 (2009)

Katsuno, Y., Suzuki, A., Sugimura, K., Okumura, K., Zineldeen, D.H., Shimada, M., Niida, H., Mizuno, T., Hanaoka, F., and Nakanishi, M. Cyclin A-Cdk1 regulates the origin firing program in mammalian cells. ***Proc. Natl. Acad. Sci.*** 106, 3184-3189 (2009)

Nagata, D., Hashimoto, Y., Nakanishi, M., Naruyama, H., Okada, S., Ando, R., Tozawa, K., and Kohri, K. Peroxisome proliferator-activated receptor-gamma and growth inhibition by its ligands in prostate cancer. ***Cancer Detect Prev.*** 32, 259-266 (2008)

Naruyama, H., Shimada, M., Niida, H., Zineldeen, D.H., Hashimoto, Y., Kohri, K., and Nakanishi, M. Essential role of Chk1 in S phase progression through regulation of RNR2 expression. ***Biochem. Biophys. Res. Commun.*** 374, 79-83 (2008)

Shimada, M. and Nakanishi, M. Checkpoints meet transcription at a novel histone milestone (H3-T11). ***Cell Cycle*** 7, 1555-1559 (2008).

Hikosaka, A., Ogawa, K., Sugiura, S., Asamoto, M., Takeshita, F., Sato, S.Y., Nakanishi, M., Kohri, K., and Shirai, T. Susceptibility of p27 kip1 knockout mice to urinary bladder carcinogenesis induced by N-butyl-N-(4-hydroxybutyl)nitrosamine may not simply be due to enhanced proliferation. ***Int. J. Cancer*** 122, 1222-1228 (2008)

Shimada, M., Niida, H., Zineldeen, D.H., Tagami, H., Tanaka, M., Saito, H., and Nakanishi, M. Chk1 is a histone H3 threonine 11 kinase that regulates DNA damage-induced transcriptional repression. ***Cell*** 132, 221-232 (2008)

Shimada, M., Yamada-Namikawa, C., Murakami-Tonami, Y., Yoshida, T., Nakanishi, M., Urano, T., and Murakami, H. Cdc2p controls the forkhead transcription factor Fkh2 by phosphorylation during sexual differentiation in fission yeast. ***EMBO J.*** 27, 132-142 (2008)

2. 学会発表

第６７回日本癌学会学術総会シンポジウム
平成２０年１０月２８日～３０日
「細胞周期と発がん」

第３１回分子生物学会年会、第８１回日本生化学学会大会合同大会シンポジウム
平成２０年１２月８日～１２日
「ＤＮＡ損傷応答における新たなヒストン修飾Ｈ３－Ｔ１１のリン酸化を介した転写制御」

H. 知的財産権の出願・登録状況（予定を含む）
1. 特許取得　　なし

2. 実用新案登録　　なし

3. その他

書籍

著者氏名	論文タイトル名	書籍全体の編集者名	書籍名	出版社名	出版地	出版年	ページ
Nakanishi, M.	Chromatin Modifications and Orchestration of Checkpoint response and Cancer	Siddik, Z.ed.	Checkpoint Controls and Targets in Cancer Therapy	Human Press.	U.S.A.	2008	Chapter 6

雑誌

発表者氏名	論文タイトル名	発表誌名	巻号	ページ	出版年
Zineldeen, D.H., Shimada, M., Niida, H., Katsuno, Y., and Nakanishi, M.	Ptpcd-1 is a novel cell cycle related phosphatase that regulates centriole duplication and cytokinesis.	***Biochem. Biophys. Res. Commun.***	380	460-466	2009
Nishizuka, M., Kishimoto, K., Kato, A., Ikawa, M., Okabe, M., Sato, R., Niida, H., Nakanishi, M., Osada, S., and Imagawa, M.	Disruption of the novel gene fad14 causes rapid postnatal death and attenuation of cell proliferation, adhesion, spreading and migration.	***Exp. Cell Res.***	315	809-819	2009
Katsuno, Y., Suzuki, A., Sugimura, K., Okumura, K., Zineldeen, D.H., Shimada, M., Niida, H., Mizuno, T., Hanaoka, F., and Nakanishi, M.	Cyclin A-Cdk1 regulates the origin firing program in mammalian cells.	***Proc. Natl. Acad. Sci.***	106	3184-3189	2009
Nagata, D., Hashimoto, Y., Nakanishi, M., Naruyama, H., Okada, S., Ando, R., Tozawa, K., and Kohri, K.	Peroxisome proliferator-activated receptor-gamma and growth inhibition by its ligands in prostate cancer.	***Cancer Detect Prev.***	32	259-266	2008
Naruyama, H., Shimada, M., Niida, H., Zineldeen, D.H., Hashimoto, Y., Kohri, K., and Nakanishi, M.	Essential role of Chk1 in S phase progression through regulation of RNR2 expression.	***Biochem. Biophys. Res. Commun.,***	374	79-83	2008

発表者氏名	論文タイトル名	発表誌名	巻号	ページ	出版年
Shimada, M. and Nakanishi, M.	Checkpoints meet transcription at a novel histone milestone (H3-T11).	***Cell Cycle***	7	1555-1559	2008
Hikosaka, A., Ogawa, K., Sugiura, S., Asamoto, M., Takeshita, F., Sato, S.Y., Nakanishi, M., Kohri, K., and Shirai, T.	Susceptibility of p27 kip1 knockout mice to urinary bladder carcinogenesis induced by N-butyl-N-(4-hydroxy butyl)nitrosamine may not simply be due to enhanced proliferation.	***Int. J. Cancer***	122	1222-1228	2008
Shimada, M., Niida, H., Zineldeen, D.H., Tagami, H., Tanaka, M., Saito, H., and Nakanishi, M.	Chk1 is a histone H3 threonine 11 kinase that regulates DNA damage-induced transcriptional repression.	***Cell***	132	221-232	2008
Shimada, M., Yamada-Namikawa, C., Murakami-Tonami, Y., Yoshida, T., Nakanishi, M., Urano, T., and Murakami, H.	Cdc2p controls the forkhead transcription factor Fkh2 by phosphorylation during sexual differentiation in fission yeast.	***EMBOJ.***	27	132-142	2008

Cyclin A–Cdk1 regulates the origin firing program in mammalian cells

Yuko Katsuno[a], Ayumi Suzuki[a], Kazuto Sugimura[b], Katsuzumi Okumura[b], Doaa H. Zineldeen[a], Midori Shimada[a], Hiroyuki Niida[a], Takeshi Mizuno[c], Fumio Hanaoka[c,d], and Makoto Nakanishi[a,1]

[a]Department of Cell Biology, Graduate School of Medical Sciences, Nagoya City University, 1 Kawasumi, Mizuho-cho, Mizuho-ku, Nagoya 467-8601, Japan; [b]Laboratory of Molecular and Cellular Biology, Graduate School of Bioresources, Mie University, 1577 Kurimamachiya-cho, Tsu, Mie 514-8507, Japan; [c]Cellular Physiology Laboratory, RIKEN Discovery Research Institute, and Solution Oriented Research for Science and Technology, Science and Technology Corporation, Wako, Saitama 351-0198, Japan; and [d]Faculty of Science, Gakushuin University, Toshima, Tokyo 171-8588, Japan

Edited by Tak Wah Mak, University of Toronto, Toronto, Canada, and approved January 12, 2009 (received for review September 18, 2008)

Somatic mammalian cells possess well-established S-phase programs with specific regions of the genome replicated at precise times. The ATR–Chk1 pathway plays a central role in these programs, but the mechanism for how Chk1 regulates origin firing remains unknown. We demonstrate here the essential role of cyclin A2–Cdk1 in the regulation of late origin firing. Activity of cyclin A2–Cdk1 was hardly detected at the onset of S phase, but it was obvious at middle to late S phase under unperturbed condition. Chk1 depletion resulted in increased expression of Cdc25A, subsequent hyperactivation of cyclin A2–Cdk1, and abnormal replication at early S phase. Hence, the ectopic expression of cyclin A2–Cdk1AF (constitutively active mutant) fusion constructs resulted in abnormal origin firing, causing the premature appearance of DNA replication at late origins at early S phase. Intriguingly, inactivation of Cdk1 in temperature-sensitive Cdk1 mutant cell lines (FT210) resulted in a prolonged S phase and inefficient activation of late origin firing even at late S phase. Our results thus suggest that cyclin A2–Cdk1 is a key regulator of S-phase programs.

Chk1 | DNA replication | molecular combing | ATR protein | checkpoint

Duplication of the eukaryotic genome is regulated by multiple elements including initiation of DNA replication, rate of fork progression, stability of replication forks, and the origin firing program (1). Replication origins are fired in small groups that are activated together within individual replication factories and thus can be visualized as foci (2). Replication origins in a single replication factory are actually comprised of several candidate origins, most of which are not normally used through the mechanism by which firing of 1 origin inhibits activation of any other Mcm2–7 complexes within that factory (3). Thus, S-phase programs appear to be regulated by 2 distinct levels of origin firing; one is the sequential activation of replicon clusters characterized as visible replication foci, and the other is the selection of 1 Mcm2–7 complex around the ORC within a single replication factory.

The DNA replication checkpoint system was reported to be involved in the origin firing program in vertebrate cells (4). In analysis using *Xenopus* egg extract, ATR/Chk1 was shown to regulate the sequential activation of early and late replication origins (5). Chk1 also regulates the density of active replication origins during S phase of avian cells (6). Therefore, ATR/Chk1 may be involved in the regulation of sequential activation of replicon clusters and selection of origins within a single replication factory. Chk1 has been shown to regulate the physiological turnover of Cdc25A and its phosphatase activity, which in turn regulates several cyclin–Cdk activities (7) that are prerequisite for origin firing throughout S phase.

In budding yeast, Clb5-dependent Cdk activity is indispensable for activation of late replication origins (8), suggesting the existence of a specific transfactors for late origin activation in other eukaryotes. In fission yeast, however, clear late origins have not been characterized (9) and replication origins fire stochastically (10, 11). As for mammals, although almost half of origins are activated equally throughout S-phase progression (12), stable subunits of chromosomes equivalent to replication foci maintain their replication timing from S phase to S phase (13).

In this article, we demonstrate that Chk1 depletion resulted in an aberrant origin firing and a hyperactivation of cyclin A2–Cdk1 at early S phase. Ectopic expression of cyclin A2–Cdk1AF induced late origin firing at early S phase, and a loss of Cdk1 activity compromised activation of late origins at late S phase. Our results thus suggested that cyclin A2–Cdk1 might function as a transregulator of late origin firing in mammals.

Results

Chk1 Depletion Results in an Aberrant Origin Firing and a Hyperactivation of Cyclin A2–Cdk1 at Early S Phase. $Chk1^{lox/-}$ mouse embryonic fibroblasts (MEFs) were infected with adenoviruses expressing either LacZ or Cre and synchronized into G_0 phase by serum starvation (14). $Chk1^{lox/-}$ and $Chk1^{del/-}$ MEFs were then stimulated by 15% serum and double-labeled with iododeoxyuridine (IdU) and chlorodeoxyuridine (CIdU) at the indicated times, and their spatiotemporal patterns of replication sites were examined. The mammalian S phase is structured so that the sequential activation of replicon clusters occurs at spatially adjacent sites (15). This spatial relationship is maintained in $Chk1^{lox/-}$ MEFs (Fig. 1*A*), where 86.6 ± 4.4 of foci showed colocalization visualized as yellow color. In contrast, colocalization was detected only at 53.9 ± 4.8 of foci in $Chk1^{del/-}$ MEFs (Fig. 1*B*), indicating that Chk1 depletion in mammals resulted in the aberrant origin firing as observed in avian cells (6). Molecular combing of single DNA molecules was performed to visualize individual origin activation, measure the fork elongation, and define replication structures (Fig. 1*C* and Fig. S1). In asynchronized $Chk1^{lox/-}$ MEFs infected with control LacZ adenoviruses interorigin spacing (90.4 kb on average) was similar to that in mock-infected cells. Chk1 depletion resulted in a clear reduction in origin spacing (34.8 kb on average)(Fig. 1*C Top*). Spatiotemporal pattern of replication sites could also be affected by fork elongation. Chk1 depletion reduced the rate of fork elongation throughout the labeling period (Fig. 1*C Middle*).

Double-labeling protocol also defines 5 classes of replication structure as described (6). Chk1 depletion resulted in a significant reduction in a proportion of consecutively elongating forks (class 1) and an increase in number of new firing initiation during the first (class 2) and second (class 4) labeling period (Fig. 1*C Bottom*). A dramatic increase in the frequency of closely-spaced active origins

Author contributions: M.N. designed research; Y.K., A.S., K.S., K.O., D.H.Z., M.S., and H.N. performed research; T.M. and F.H. contributed new reagents/analytic tools; Y.K., K.S., and M.N. analyzed data; and Y.K. and M.N. wrote the paper.

The authors declare no conflict of interest.

This article is a PNAS Direct Submission.

[1]To whom correspondence should be addressed. E-mail: mkt-naka@med.nagoya-cu.ac.jp.

This article contains supporting information online at www.pnas.org/cgi/content/full/0809350106/DCSupplemental.

www.pnas.org/cgi/doi/10.1073/pnas.0809350106

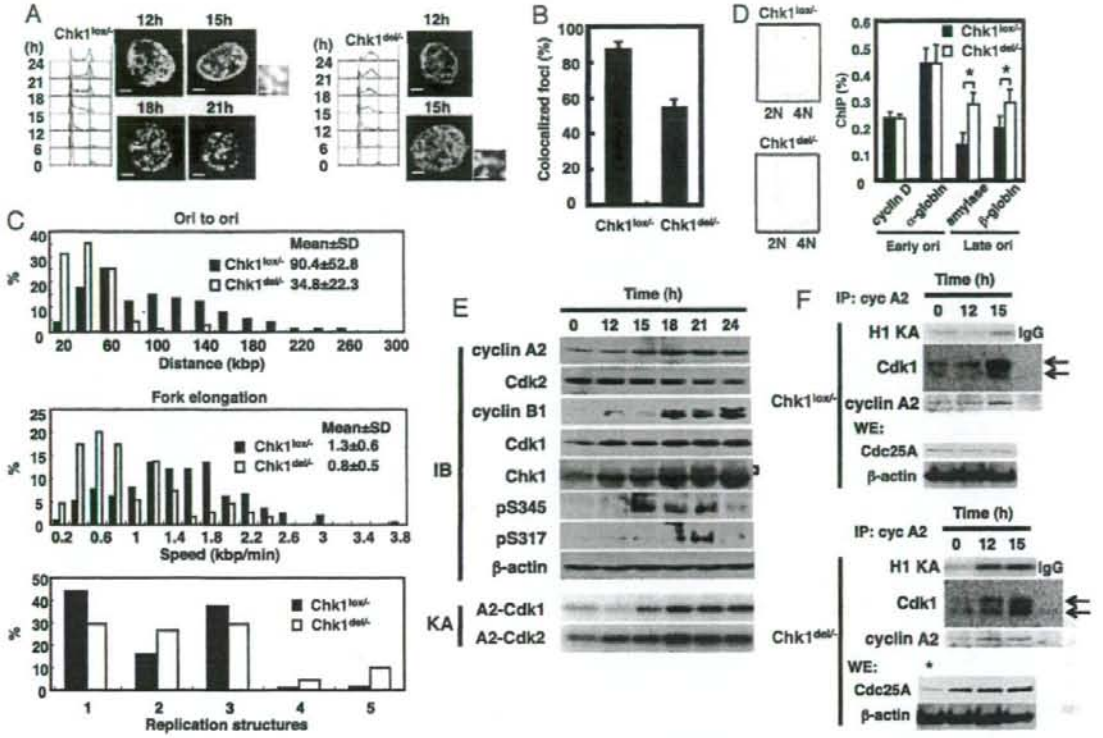

Fig. 1. Chk1 depletion results in an aberrant S-phase program and an activation of cyclin A2–Cdk1 at early S phase. (*A*) Chk1$^{lox/-}$ and Chk1$^{del/-}$ MEFs were synchronized at quiescence by serum starvation and then released by the addition of 15% serum. Cells were harvested at the indicated times, and their cell cycle distributions were analyzed by FACS. Replication sites were pulse-labeled for 15 min with 100 μM IdU and then for 15 min with 100 μM CldU, and analyzed with a Zeiss LSM5 confocal fluorescence microscope. Typical patterns of replication sites at the indicated times are presented. High-power details are from the boxed areas shown. (Scale bars: 5 and 0.5 μm in detail.) (*B*) Colocalization of IdU and CldU foci in Chk1$^{lox/-}$ and Chk1$^{del/-}$ MEFs. Relative colocalization of IdU and CldU foci was determined as a percentage of total foci in both cells ($n > 30$). Data are means ± SD of at least 3 independent experiments. (*C*) Asynchronized Chk1$^{lox/-}$ MEFs were infected with the indicated adenoviruses and double-labeled with IdU and CldU before harvesting at 28 h after infection. Replication structures were visualized by means of dynamic molecular combing. Adjacent origins in replicon clusters (Ori to ori), fork elongation, and replication structure defined by ref. 6 were determined ($n > 100$). Frequency histograms show the distribution of separation in distance (kbp), speed (kbp/min), and replication structure (1, elongating fork; 2, fork growing from 1 ori; 3, terminal fusions; 4, isolated; 5, interspersed). (*D*) Asynchronized Chk1$^{lox/-}$ MEFs were infected with adenoviruses expressing either LacZ or Cre. Cells were labeled with BrdU for 1 h before harvesting at 28 h after infection, and the cell cycle profiles were then analyzed by FACS. Early S-phase fraction indicated by bars was sorted, and nascent DNA was enriched by immunoprecipitation using α-BrdU. The indicated genes were amplified by quantitative PCR, and the results are presented as a percentage of mtDNA. Data are means ± SD of at least 3 independent experiments. Statistical significance was assessed by Student's *t* test (*, $P < 0.01$). (*E*) Synchronized Chk1$^{lox/-}$ MEFs as in *A* were harvested at the indicated times, and the lysates were subjected to immunoblotting by using the indicated antibodies or to an in vitro kinase assay (KA) for cyclin A2–Cdk1 and cyclin A2–Cdk2 with HH1 (2 μg) as a substrate. (*F*) Synchronized Chk1$^{lox/-}$ and Chk1$^{del/-}$ MEFs as in *A* were harvested at the indicated times, and the lysates were immunoprecipitated by using α-cyclin A2 antibodies after 3 times preabsorbance with α-Cdk2. The resultant immunoprecipitates (IP: cyclin A2) or whole-cell extracts (WE) were subjected to immunoblotting or in vitro kinase assay as in *E*. Arrows indicate the fast (active) or slow (inactive) migrated bands of Cdk1. An asterisk represents cell lysates from Chk1$^{lox/-}$ MEFs at 15 h.

(class 5) was observed. These observations suggest that loss of Chk1 frequently stalls and collapses active forks.

We next examined whether Chk1 regulates global sites of DNA synthesis by quantitative ChIP using FACS-based cell sorting (16). To avoid unexpected effects from gross changes in cell cycle profile on this analysis, we analyzed Chk1$^{del/-}$ MEFs 28 h after adenoviral infection, the time at which Chk1 was completely depleted, but the cell cycle profile was almost the same as that of Chk1$^{lox/-}$ cells (Fig. 1*D*). Cells from the first third of S phase were collected (Fig. 1*D Left*). Nascent (BrdU-containing) DNA was enriched by immunoprecipitation using α-BrdU antibodies and amplified by quantitative PCR with specific primers for cyclin D and α-globin for early-replicating DNA and primers for amylase and β-globin for late-replicating DNA. We also monitored amplification of mtDNA as a control, which replicates throughout the cell cycle and is equally represented in nascent DNA preparations (16, 17). The relative amounts of early replication (cyclin D and α-globin) in Chk1$^{del/-}$ MEFs were almost the same as those in Chk1$^{lox/-}$ cells, whereas those of late replication (amylase and β-globin) in Chk1$^{del/-}$ MEFs were significantly higher than those in Chk1$^{lox/-}$ cells (Fig. 1*D Right*). Given that 1 cell possesses ≈1,000 copies of mitochondrial genome, but they replicate throughout the cell cycle, relative amplification of nascent DNA (≈0.3) for early and late origins appeared consistent.

Chk1 is phosphorylated during unperturbed S phase (18, 19), which regulates the activity and stability of Cdc25 phosphatases, leading to the inactivation of Cdks through increased phosphorylation of their Y15 residues (20). Thus, we speculated that Chk1

regulates origin firing program through affecting certain cyclin–Cdks activities. The band corresponding to Chk1 was shifted upward at 15 h and thereafter. This band shift was reversed by phosphatase treatment, indicating that the modification was caused by phosphorylation. Chk1 phosphorylation was also confirmed by using phospho-specific antibodies to Chk1 at Ser-317 and Ser-345 (Fig. 1*E*).

Cyclin A2–Cdk1 activity was first detected at 15 h (middle S phase) and increases thereafter. Cyclin A2–Cdk2 was detected at 6 h (early S phase) and reached maximum at 18 h (Fig. 1*E* and Fig. S2*A*). These results are consistent with the recent report that cyclin A2 starts to form a complex with Cdk1 at mid-S phase (21). Cyclin A2–Cdk1 activity was detected earlier and enhanced in $Chk1^{del/-}$ MEFs when compared with $Chk1^{lox/-}$ MEFs (Fig. 1*F*), where immunodepletion of Cdk2 was equally achieved in both cyclin A2 immunoprecipitates (Fig. S2*B*). Cyclin A2–Cdk2 activity was not apparently affected by Chk1 depletion (Fig. S2*A*). Intriguingly, the amount of Cdc25A was highly elevated in $Chk1^{del/-}$ MEFs. Consistent with this increase in amount of Cdc25A, fast mobility band (active; Y15 dephosphorylation) and slow band (inactive; Y15 phosphorylation) of Cdk1 protein were dominant in those from $Chk1^{del/-}$ MEFs and $Chk1^{lox/-}$ MEFs, respectively (Fig. 1*F*). Specificity of cyclin A2–Cdk1 activity was confirmed by Cdk1 knockdown experiment, where cyclin A2–Cdk1 activities in both MEFs were significantly reduced after Cdk1 depletion (Fig. S3). To further confirm the functional interaction between Chk1 and cyclin A2–Cdk1, $Chk1^{lox/-}$ MEFs were treated with UV light, which phosphorylated Chk1 in an ATR-dependent manner. Chk1 phosphorylation was correlated with the reduction of Cdc25A, the appearance of slow mobility band of Cdk1 protein, and inhibition of cyclin A2–Cdk1 activity (Fig. S4). Taken together, cyclin A2–Cdk1 is likely to be a target of Chk1 through regulation of Cdc25A.

Aberrant Origin Firing in Cells Expressing Cyclin A2–Cdk1AF Fusion Protein. To examine the role of each cyclin–Cdk complex in the origin firing program, we generated a cyclin A2–Cdk1 fusion construct. Because cyclin–Cdk activities are regulated mainly by the phosphorylation of Y15, we generated a constitutively active mutant (CdkAF) in which residues at inhibitory phosphorylation sites were replaced with alanine and phenylalanine and therefore the mutant was not affected by the Chk1–Cdc25 pathway. Recombinant cyclin A2–Cdk2AF, cyclin A2–Cdk1AF, and cyclin B1–Cdk1AF complexes and the fusion proteins were examined for their enzymatic kinetics by using histone H1 (HH1) and lamin B as substrates. Dose-dependent increases in activities of both cyclin–Cdks complex and their fusion proteins were observed (Fig. 2*A*). The kinetic values of these complexes were the same as those of the fusion proteins (Table S1).

Expression of cyclin B1–Cdk1AF, but not cyclin A2–Cdk2AF or cyclin A2–Cdk1AF, induced γH2AX foci in HeLa cells (Fig. 2*B*). Amounts of cyclin B1–Cdk1AF, cyclin A2–Cdk1, and cyclin A2–Cdk2 fusion proteins expressed at 24 h after infection were almost equal to endogenous Cdk1 and Cdk2 proteins, respectively (Fig. 2*C* and Fig. S5). Again, γH2AX was not detected by immunoblotting in cells expressing cyclin A2–Cdk1 or cyclin A2–Cdk2 fusion protein.

Expression of cyclin A2–Cdk1AF and cyclin A2–Cdk2AF fusion protein at the endogenous level did not appear to affect the gross progression of S phase (Fig. 3*A*) although they arrested the cell cycle at M phase because of their inability to be degraded by APC-C at mitosis and thus mitotic exit was inhibited. The expression of cyclin A2–Cdk1AF fusion protein caused the appearance of late replication sites during early S phase when cells were double-labeled with IdU and CIdU (Fig. 3*B*). Dynamic molecular combing revealed that expression of cyclin A2–Cdk1AF fusion protein reduced origin spacing (75.0 kb on average), whereas that of cyclin A2–Cdk2AF

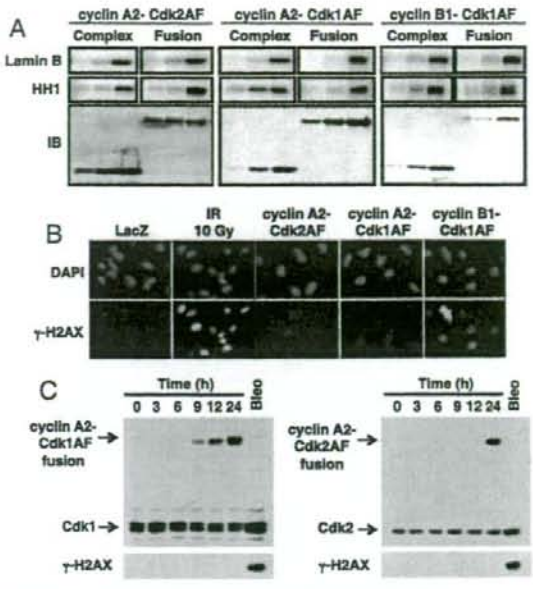

Fig. 2. Enzymatic kinetics of cyclin–Cdk fusion proteins. (*A*) Baculoviruses expressing cyclin A2 together with those expressing Cdk2 or Cdk1 (Complex) or those expressing cyclin A2–Cdk2, cyclin A2–Cdk1, or cyclin B1–Cdk1 fusion protein (Fusion) were used to infect insect cells. Their complexes or fusion proteins were purified and subjected to an in vitro kinase assay using lamin B (2 μg) or HH1 (2 μg) as a substrate or subjected to immunoblotting by using Cdk2 or Cdk1 antibodies (IB). (*B*) HeLa cells were infected with adenoviruses expressing the indicated proteins 24 h before fixing and immunostained with α-γH2AX antibodies. Their nuclei were counterstained with DAPI. As a positive control, cells infected with adenoviruses expressing LacZ were treated with IR (10 Gy). (Magnifications: 100×.) (*C*) HeLa cells were infected with adenoviruses expressing either cyclin A2-Cdk1AF or cyclin A2-Cdk2AF fusion proteins. Cells were harvested at the indicated times, and the lysates were subjected to immunoblotting using α-Cdk1 (*Upper Left*), α-Cdk2 (*Upper Right*), or α-γH2AX antibodies (*Lower*). As a control, HeLa cells were treated with bleomycin for 24 h (20 μg/mL).

did not (113.0 kb on average)(Fig. 3*C Top* and Fig. S6). Unlike Chk1 depletion, expression of cyclin A2–Cdk2AF did not cause significant changes in the proportion of abnormal replication structures (Fig. 3*C Bottom*). Taken together, these results suggested that cyclin A2–Cdk1 had a specific role in the origin firing program.

ChIP analysis revealed that considerable enrichment of early- and late-replicating DNA was specifically observed in the early and late S-phase fractions of control LacZ cells, respectively (Fig. 3*D*). Ectopic expression of cyclin A2–Cdk1AF resulted in the dramatic increase in replication of late origins in early S-phase fractions, but that of cyclin A2–Cdk2AF did not apparently affect it.

Cdk1 Is Required for Proper Timing of Origin Firing. FT210 cells possess a temperature-sensitive Cdk1 gene product (22). FACS analysis revealed a 2-h-longer S phase in FT210 cells compared with the parental FM3A cells (Fig. 4*A*). S-phase progression of FT210 cells at a permissive temperature was almost the same as that of FM3A cells. The progression of the spatiotemporal pattern of DNA replication sites in FM3A at the nonpermissive temperature was almost the same as in HeLa cells or MEFs. In contrast, the specific pattern of DNA replication sites observed in late S phase showing a few large internal foci was hardly detected in FT210 cells even at late S phase at nonpermissive temperature (Fig. 4*A*). Loss of Cdk1

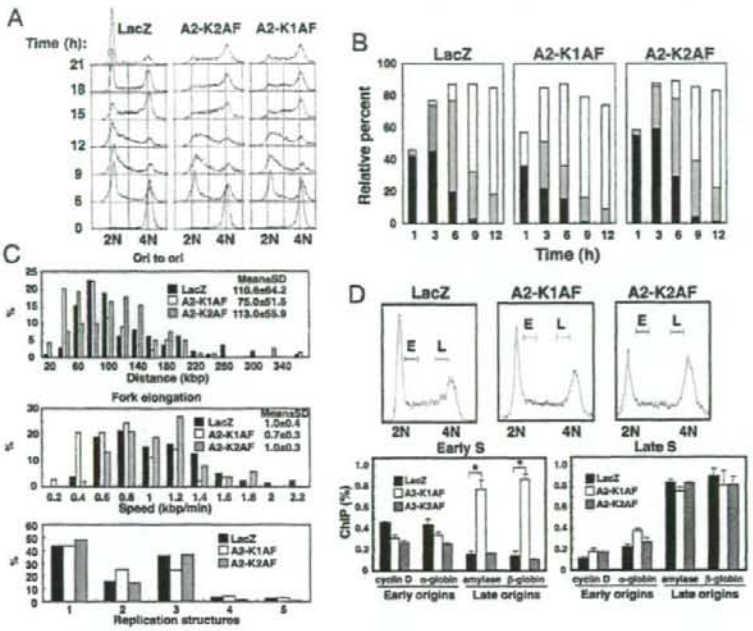

Fig. 3. Ectopic expression of cyclin A2-Cdk1AF, but not cyclin A2–Cdk2AF resulted in an aberrant temporal regulation of origin firing. (*A*) HeLa cells were synchronized by thymidine (2 mM, 24 h)/release period (6 h)/nocodazole (0.1 μg/mL, 12 h) and infected with adenoviruses expressing either cyclin A2–Cdk2AF, cyclin A2–Cdk1AF, or LacZ (control) 12 h before nocodazole washout (time 0). Cells were harvested at the indicated times, and their cell cycle profiles were analyzed by FACS. (*B*) HeLa cells were infected with the indicated adenoviruses 24 h before mimosine (0.6 mM, 16 h) washout (time 0). Replication sites were pulse-labeled for 15 min with IdU (100 μM) and then for 15 min with CldU (100 μM) before harvesting at the indicated times. The number of replication sites of each pattern was counted, and the relative percentage of the total number of cells ($n > 300$) is indicated. Black bars represent the early pattern, gray bars represent the middle pattern, and white bars represent the late pattern. Data are means of at least 3 independent experiments. (*C*) Asynchronous HeLa cells were infected with the indicated adenoviruses. Cells were harvested 24 h after infection and subjected to molecular combing. Adjacent origins in replicon clusters (Ori to ori), fork elongation, and replication structure were determined ($n > 100$) as in Fig. 1*C*. (*D*) Asynchronous HeLa cells infected with the indicated adenoviruses were pulse-labeled with BrdU before harvesting cells 24 h after infection. S-phase cells were then sorted into early (E) or late (L) fractions (*Upper*). The sorted cells were collected, and replication firing at the indicated origins was analyzed by ChIP analysis (*Lower*) as in Fig. 1*D*. Data are means ± SD of at least 3 independent experiments. Statistical significance was assessed by Student's *t* test (*, $P < 0.01$).

resulted in a significant increase in origin spacing (104.7 kb on average) when compared with control cells (78.6 kb on average) (Fig. 4*B Top* and Fig. S6). Loss of Cdk1 did not cause changes in the proportion of replication structures, further supporting the notion that Cdk1 is not involved in the stabilization of replication forks.

ChIP analysis revealed that replication patterns of early S-phase fractions in both cells were very similar, whereas replication of late origins in late S-phase fraction from FT210 cells was specifically impaired (Fig. 5*A Right*). Cdk2 activity during S phase in FT210 cells appeared the same as that in FM3A cells (Fig. S7). Collectively, these results suggested that Cdk1 activity is involved in the proper timing of late origin firing.

Finally, we attempted to determine the molecular basis by which cyclin A2–Cdk1 regulates origin firing program. In *Xenopus* and yeast systems, it was reported that cyclins, Cdk1 specifically, interact with the origin recognition complexes (ORCs) (23, 24). To examine whether the specific interaction of Cdk1 to ORCs is conserved among mammals, we performed ChIP analysis with α-Cdk1 and α-Cdk2 antibodies. Both Cdk1 and Cdk2 were detected at genes replicating early, whereas Cdk1 was specifically detected at genes replicating late (Fig. 5*B*). Relative binding of Cdk1 and Cdk2 appeared somewhat low, presumably because of an asynchronous cell cycle. These results suggested that the specific binding of Cdk1 to late origins may also be involved in the regulation of origin firing programs.

Discussion

Conditional Chk1 knockout MEFs revealed that Chk1 plays an important role in the regulation of origin firing at 2 distinct levels in mammals, namely activation of origins within a single replication factory and activation of replicon clusters (Fig. 1 *A–D*). Consistent with our observations, it was very recently proposed that Chk1 suppresses initiation in both inactive, later-firing clusters and active clusters, and the former is more strongly repressed (25). We then successfully showed that expression of cyclinA2–Cdk1AF fusion proteins activated origin firing at both levels as Chk1 depletion did (Fig. 3 *B–D*). The expression patterns of Cdk1 and cyclins during S phase and the enhancement of their activities in response to Chk1 depletion are also consistent with our conclusions (Fig. 1 *E* and *F*). The most striking evidence for the involvement of Cdk1 in DNA replication is the fact that inactivation of Cdk1 in mammalian cells resulted in a prolonged S phase accompanied by ineffective firing of late replicon clusters and reduced the density of active origins (Figs. 4 and 5*A*). Although our present results clearly demonstrate that cyclin A2–Cdk1 is involved in the regulation of late origin firing, functioning downstream of Chk1, we cannot rule out the possibility that cyclin A2–Cdk2 has a redundant function. Hochegger *et al.* (26) reported that Cdk1 activity was essential for DNA replication initiation when Cdk2 was depleted in chicken DT40 cells. When Cdk2 was present, Cdk1 inhibition did not delay S phase or block centrosome duplication. In this regard, DNA replication in DT40 cells appears complete within a shorter period (8 h) when compared with mammalian cells (10 h at 37 °C). Therefore, it is possible that DT40 cells possess a strong Cdk2 activity, presumably because of a loss of functional p53 that reduces the level of p21 Cdk inhibitor, and the high Cdk2 activity may compensate for the loss of Cdk1 activity in the context of S-phase control. In agreement with this notion, both Cdk1 and Cdk2 were recently reported to be involved in the control of DNA replication and replication origin firing under unperturbed S phase in the *Xenopus* system (27). It was also suggested that Cdk1 and Cdk2 must have different activities toward the genuine substrates involved in DNA replication although one kinase alone is minimally sufficient to promote substantial DNA replication.

Neither cyclin A2–Cdk1 nor cyclin A2–Cdk2 appeared to be involved in the stabilization of replication forks during S phase

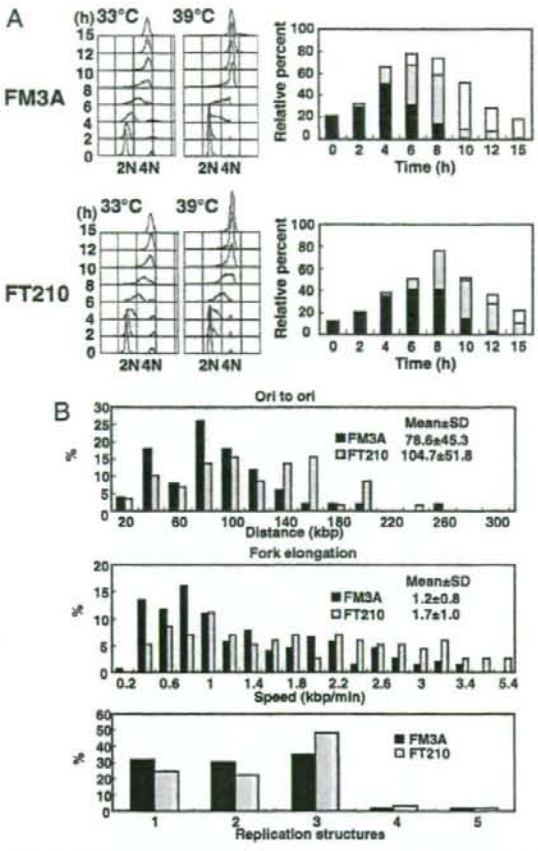

Fig. 4. Prolonged S phase in temperature-sensitive Cdk1 mutant FT210 cells. (*A*) FT210 and the parental FM3A cells were synchronized at M phase by nocodazole (0.5 μg/mL, 16 h) and then released at an either permissive (33 °C) or nonpermissive (39 °C) temperatures. Cells were then harvested 3 h after release (time 0) and at various times thereafter. Their replication sites were analyzed ($n > 300$) as in Fig. 3*B*. Data are means of at least 3 independent experiments. (*B*) Asynchronized FM3A and FT210 cells were shifted at 39 °C for 4 h. Cells were then harvested and subjected to molecular combing. Adjacent origins in replicon clusters (Ori to ori), fork elongation, and replication structure were determined ($n > 100$) as in Fig. 1*C*.

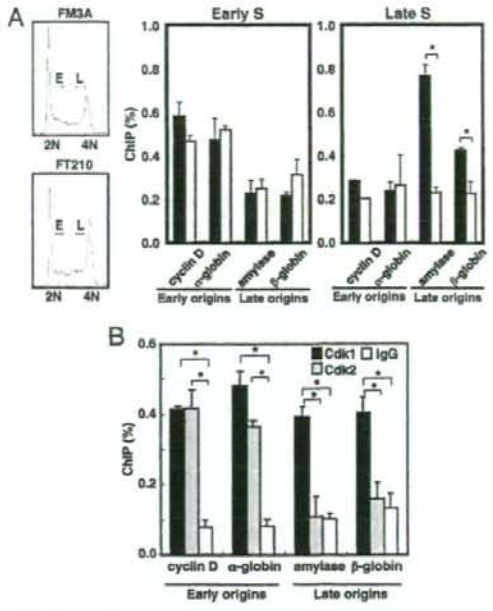

Fig. 5. Impaired late origin firing in temperature-sensitive Cdk1 mutant FT210 cells. (*A*) Asynchronous FM3A and FT210 cells were shifted at 39 °C for 4 h. Cells were pulse-labeled with BrdU (25 μM) for 1 h and sorted into early (E) or late (L) fractions. Replication firing at the indicated origins was analyzed by ChIP analysis as in Fig. 3*D*. Data are means ± SD of at least 3 independent experiments. Statistical significance was assessed by Student's *t* test (*, $P < 0.01$). Filled bars indicate FM3A cells; empty bars indicate FT210 cells. (*B*) Asynchronous FM3A cells were cultured at 33 °C and harvested. Cell lysates were subjected to ChIP analysis as described in *Materials and Methods*. Data are means ± SD of at least 3 independent experiments. Statistical significance was assessed by Student's *t* test (*, $P < 0.01$).

when replication structures were assessed by dynamic molecular combing technology (Fig. 3*C*). This idea was further supported by the observations that ectopic expression of cyclin A2–Cdk1AF and cyclin A2–Cdk2AF failed to induce DNA damage (Fig. 2 *B* and *C*). These findings present a clear contrast to the case with Chk1 depletion in which stability of replication forks during S phase was strikingly reduced. Therefore, Chk1 likely regulates the fork stability in a manner independent of cyclin–Cdk activities.

Cdk activities have both positive and negative roles during S phase, namely to initiate DNA synthesis and prevent rereplication. A quantitative model has proposed for explain the biphasic effects of Cdks (28). In addition to a quantitative model, the accessibility of Cdk to substrates could play a role in the regulation of the S-phase program. Studies in *Xenopus* and yeast systems suggested that Cdk1 specifically interacts with ORC and phosphorylates the components more efficiently than Cdk2 although this interaction is proposed to be involved in prevention of rereplication (23, 24). We found that Cdk1 could bind to both early and late origins but Cdk2 failed to bind to late origins (Fig. 5*B*). Thus, Cdk1 could potentially activate early origin firing. This notion is supported by the fact that Cdk1 could complement the Cdk2 function of S-phase initiation in Cdk2-depleted cells (26). However, because neither ectopic expression of cyclin A2–Cdk2AF nor cyclin A2–Cdk1AF resulted in the further enhancement of early origin activation (Fig. 3*D*), activation of endogenous cyclin A/E–Cdk2 at the S-phase onset appeared to be sufficient for early origin firing. Furthermore, given that the majority of endogenous Cdk1 and Cdk2 existed in soluble fractions (Fig. S8), the origin activation program appeared to be regulated not only by induction of Cdks and their binding to prereplicative complex components, but also by alternative ways such as complex formation with cyclins or regulation of inhibitory phosphorylation of Cdks. In this regard, it was very recently reported that Cdk1 started to form a complex with cyclin A2 after cyclin A2–Cdk2 complexes reached a plateau in mid S phase (21). Taken together, our results suggest that cyclin A2–Cdk1 may regulate origin firing program through both its specific accessibility to late origins and regulation of Cdk1 activity at late S phase.

In conclusion, the present results indicate that ATR/Chk1–cyclin A2–Cdk1 controls the activation of late replication origins and the density of active origins in mammals. Similar regulation was reported in a budding yeast system in which Clb5–Cdk1 was required for late origin firing (8). Taken together, these results suggest the existence of conserved mechanisms for the temporal program of origin activation among a number of eukaryotes.

Materials and Methods

Antibodies. Antibodies used in this study were as follows: α-CDK2 (sc-748; Santa Cruz), α-Cyclin A2 (sc-751; Santa Cruz), α-Cdc2 (sc-54; Santa Cruz), α-Cyclin B1 (sc-245; Santa Cruz), rat α-BrdU (ab6326; Abcam), mouse α-BrdU (347580; BD), α-γH2AX (05-636; Upstate), α-rabbit IgG HRP (NA934; GE Healthcare), α-mouse IgG HRP (NA931; GE Healthcare), Alexa Fluor 555-conjugated goat α-mouse IgG (A-21422; Invitrogen), and Alexa Fluor 488-conjugated rabbit α-rat IgG (A-21210; Invitrogen).

Cell Culture and Double Labeling with IdU and CldU. HeLa cells, Chk1$^{low/-}$ MEFs, Chk1$^{del/-}$ MEFs, FM3A, and FT210 cells were cultured as described (14, 29). For analyses of origin firing programs, cells were incubated with 100 μM IdU for 15 min, then 100 μM CldU for 15 min, fixed with 4% paraformaldehyde, and permabilized. Cellular DNA was denatured in 1.5 M HCl and stained as reported (6). The spatiotemporal patterns of replication were analyzed by counting at least 300 cells by 2 individuals under blinded conditions.

Dynamic Molecular Combing and Immunofluorescent Detection. Genomic DNA was prepared and combed onto the silanated cover slips as described (30) with modifications as detailed (31). A total of 2×10^6 cells were pulse-labeled for 20 min with 100 μM IdU, washed with PBS twice, and pulse-labeled for 20 min with 100 μM CldU. For preparation of genomic DNA, to remove the mitochondrial genome the nuclei were extracted with buffer A [250 mM sucrose, 20 mM Hepes (pH 7.5), 10 mM KCl, 1.5 mM $MgCl_2$, 1 mM EDTA (pH 8.0), 1 mM EGTA (pH 6.8), 1 mM DTT, 0.1 mM PMSF] before resuspension into low-melting point agarose. Combed DNA molecules were heat-denatured in 50% formamide, 2 × SSC at 72 °C for 12 min. For immunodetection of labeled DNA, denatured DNA molecules were incubated with mouse α-BrdU mAb (1:5) and rat α-BrdU mAb (1:25) for 1 h at 37°C. After washing with PBS and 0.05% Tween 20 for 5 min 3 times, DNA molecules were incubated with Alexa Fluor 555-conjugated goat α-mouse IgG (1:500) and Alexa Fluor 488-conjugated rabbit α-rat IgG (1:500) for 30 min at 37°C. All antibodies were diluted in blocking solution [1% (wt/vol) blocking reagent in PBS, 0.05% Tween 20]. After washing with PBS and 0.05% Tween 20 for 5 min 3 times, coverslips were mounted in VECTASHIELD (Vector Laboratories). To estimate the extension of DNA molecules, coverslips were prepared with λ-DNA, and then the DNA molecules were stained with 6.7 mM YOYO-1 at 25°C for 1 h. YOYO-1-stained DNA molecules measured 21 ± 0.9 μm. As the virus genome is 48.5 kbp, the extension of DNA molecules is 2.32 ± 0.11 kbp/μm. DNA fibers were examined with a Zeiss Axioplan 2 MOT with a 63X Plan-APOCHROMAT (NA 1.4) objective lens, equipped with MicroMAX CCD camera (Princeton Instruments). Fluorescent signals were measured by using MetaMorph version 6.1 software (Universal Imaging).

Construction of Cyclin A2–Cdk1, Cyclin A2–Cdk2, and Cyclin B1–Cdk1 Fusion Vectors. For subcloning of full-length mouse Cdk1 and Cdk1AF, either cDNAs from mouse MEFs or pcDNA3.1Cdk1AF were used as a template. The PCR products were digested with EcoRI and NotI and subcloned into pcDNA3.1Myc/HisA vector (Invitrogen). For subcloning of full-length mouse Cdk2 and Cdk2AF, either cDNAs from mouse MEFs or pcDNA3.1Cdk2AF were used as a template. For preparation of cyclin A2–Cdk1, cyclin A2–Cdk2, and cyclin B1–Cdk1 fusion constructs, sets of primers and mouse cDNA derived from MEFs as a template were used. The PCR products were digested with BamHI and EcoRI and subcloned into pcDNA3.1Cdk1Myc/HisA or pcDNA3.1Cdk2Myc/HisA vectors. The primer sets used are listed in Table S1.

Purification of Recombinant Cyclin–Cdk Fusion Proteins. pcDNA3.1cyclin A2–Cdk1, pcDNA3.1cyclin A2–Cdk2, pcDNA3.1cyclin B1–Cdk1, and their AF mutants were digested with BamHI and PmeI. The fragments were subcloned into pVL1392 vector and transfected into Sf9 cells. Sf9 cells infected with baculoviruses expressing cyclin–Cdk fusion proteins or coinfected with the individual cyclins and Cdks were lysed with immunoprecipitation kinase buffer (7) containing a mixture of protease inhibitors. The fusion proteins and cyclin–Cdk complexes were purified by ProBond Resin (Invitrogen) and used for the in vitro kinase assay.

Preparation of Adenoviruses Expressing Cyclin–Cdk Fusion Proteins. The BamHI–PmeI fragments of cyclin–Cdk fusion constructs were subcloned into pENTER vector (Invitrogen) predigested with BamHI and EcoRV. pENTERcyclin–Cdks and pENTERcyclin–CdkAFs were then subcloned into pAdCMV vectors according to the manufacturer's instructions (Invitrogen). pAdcyclin–Cdks and pAdcyclin–CdkAFs were transfected into 293A cells (Invitrogen).

ChIP Assay. Asynchronized Chk1$^{low/-}$ MEFs, Chk1$^{del/-}$ MEFs, HeLa cells infected with adenoviruses expressing cyclin A2–Cdk1AF or cyclin A2–Cdk2AF, and mouse FM3A or FT210 cells were labeled with 25 μM BrdU before cell sorting. Cells were then sorted into early and late S-phase fractions by using a cell sorter (BD). At least 60,000 cells were collected during each phase and used for the chromatin preparation. Nascent DNA was enriched by immunoprecipitation using α-BrdU antibodies as reported (16) and subjected to quantitative PCR with the ABI PRISM7000 system using Power SYBR Green PCR Master Mix (Applied Biosystems). Primers used for PCR are listed in Table S1. As a control, mtDNA in BrdU-containing DNA was also amplified, and the results were presented as a percentage of mtDNA. For Cdk1 and Cdk2 bindings to origins, FM3A cells were cultured at 33 °C, and ChIP analysis was performed with α-Cdk1 and α-Cdk2 antibodies as described (14). The results were presented as a percentage of input.

ACKNOWLEDGMENTS. We thank Dr. C. Namikawa-Yamada, Mr. K. Murata, and Miss H. Kojima for technical assistance. This work was supported in part by the Ministry of Education, Science, Sports, and Culture of Japan through a Grant-in-Aid of Scientific Research (to M.N.).

1. Machida YJ, Hamlin JL, Dutta A (2005) Right place, right time, and only once: Replication. *Cell* 123:13–24.
2. Jackson DA (1995) Nuclear organization: Uniting replication foci, chromatin domains, and chromosome structure. *BioEssays* 17:587–591.
3. Woodward AM, *et al.* (2006) Excess Mcm2–7 license dormant origins of replication that can be used under conditions of replicative stress. *J Cell Biol* 173:673–683.
4. Shechter D, Gautier J (2005) ATM and ATR check in on origins: A dynamic model for origin selection and activation. *Cell Cycle* 4:235–238.
5. Shechter D, Costanzo V, Gautier J (2004) ATR and ATM regulate the timing of DNA replication origin firing. *Nat Cell Biol* 6:648–655.
6. Maya-Mendoza A, Petermann E, Gillespie DA, Caldecott KW, Jackson DA (2007) Chk1 regulates the density of active replication origins during the vertebrate S phase. *EMBO J* 26:2719–2731.
7. Niida H, *et al.* (2005) Depletion of Chk1 leads to premature activation of Cdc2-cyclin B and mitotic catastrophe. *J Biol Chem* 280:39246–39252.
8. Donaldson AD, *et al.* (1998) CLB5-dependent activation of late replication origins in *S. cerevisiae*. *Mol Cell* 2:173–182.
9. Heichinger C, Penkett CJ, Bahler J, Nurse P (2006) Genomewide characterization of fission yeast DNA replication origins. *EMBO J* 25:5171–5179.
10. Dai J, Chuang RY, Kelly TJ (2005) DNA replication origins in the *Schizosaccharomyces pombe* genome. *Proc Natl Acad Sci USA* 102:337–342.
11. Patel PK, Arcangioli B, Baker SP, Bensimon A, Rhind N (2006) DNA replication origins fire stochastically in fission yeast. *Mol Biol Cell* 17:308–316.
12. Jeon Y, *et al.* (2005) Temporal profile of replication of human chromosomes. *Proc Natl Acad Sci USA* 102:6419–6424.
13. Sadoni N, Cardoso MC, Stelzer EH, Leonhardt H, Zink D (2004) Stable chromosomal units determine the spatial and temporal organization of DNA replication. *J Cell Sci* 117:5353–5365.
14. Shimada M, *et al.* (2008) Chk1 is a histone H3 threonine 11 kinase that regulates DNA damage-induced transcriptional repression. *Cell* 132:221–232.
15. O'Keefe RT, Henderson SC, Spector DL (1992) Dynamic organization of DNA replication in mammalian cell nuclei: Spatially and temporally defined replication of chromosome-specific α-satellite DNA sequences. *J Cell Biol* 116:1095–1110.
16. Hiratani I, Leskovar A, Gilbert DM (2004) Differentiation-induced replication-timing changes are restricted to AT-rich/long interspersed nuclear element (LINE)-rich isochores. *Proc Natl Acad Sci USA* 101:16861–16866.
17. Aladjem MI, *et al.* (2002) Replication initiation patterns in the β-globin loci of totipotent and differentiated murine cells: Evidence for multiple initiation regions. *Mol Cell Biol* 22:442–452.
18. Jiang K, *et al.* (2003) Regulation of Chk1 includes chromatin association and 14–3-3 binding following phosphorylation on Ser-345. *J Biol Chem* 278:25207–25217.
19. Niida H, Katsuno Y, Banerjee B, Hande MP, Nakanishi M (2007) Specific role of Chk1 phosphorylations in cell survival and checkpoint activation. *Mol Cell Biol* 27:2572–2581.
20. Bartek J, Lukas J (2003) Chk1 and Chk2 kinases in checkpoint control and cancer. *Cancer Cell* 3:421–429.
21. Merrick KA, *et al.* (2008) Distinct activation pathways confer cyclin-binding specificity on cdk1 and cdk2 in human cells. *Mol Cell* 32:662–672.
22. Th'ng JP, *et al.* (1990) The FT210 cell line is a mouse G_2 phase mutant with a temperature-sensitive CDC2 gene product. *Cell* 63:313–324.
23. Romanowski P, *et al.* (2000) Interaction of *Xenopus* Cdc2 × cyclin A1 with the origin recognition complex. *J Biol Chem* 275:4239–4243.
24. Wuarin J, Buck V, Nurse P, Millar JB (2002) Stable association of mitotic cyclin B/Cdc2 to replication origins prevents endoreduplication. *Cell* 111:419–431.
25. Ge XQ, Jackson DA, Blow JJ (2007) Dormant origins licensed by excess Mcm2–7 are required for human cells to survive replicative stress. *Genes Dev* 21:3331–3341.
26. Hochegger H, *et al.* (2007) An essential role for Cdk1 in S phase control is revealed via chemical genetics in vertebrate cells. *J Cell Biol* 178:257–268.
27. Krasinska L, *et al.* (2008) Cdk1 and Cdk2 activity levels determine the efficiency of replication origin firing in *Xenopus*. *EMBO J* 27:758–769.
28. Porter AC (2008) Preventing DNA overreplication: A Cdk perspective. *Cell Div* 3:3.
29. Fujita M, *et al.* (1998) Cell cycle- and chromatin binding state-dependent phosphorylation of human MCM heterohexameric complexes: A role for cdc2 kinase. *J Biol Chem* 273:17095–17101.
30. Michalet X, *et al.* (1997) Dynamic molecular combing: Stretching the whole human genome for high-resolution studies. *Science* 277:1518–1523.
31. Sugimura K, Takebayashi S, Taguchi H, Takeda S, Okumura K (2008) PARP-1 ensures regulation of replication fork progression by homologous recombination on damaged DNA. *J Cell Biol* 183:1203–1212.

EXPERIMENTAL CELL RESEARCH 315 (2009) 609–619

available at www.sciencedirect.com

ScienceDirect

www.elsevier.com/locate/yexcr

Research Article

Disruption of the novel gene *fad104* causes rapid postnatal death and attenuation of cell proliferation, adhesion, spreading and migration

Makoto Nishizuka[a], *Keishi Kishimoto*[a], *Ayumi Kato*[a], *Masahito Ikawa*[b], *Masaru Okabe*[b], *Ryuichiro Sato*[c], *Hiroyuki Niida*[d], *Makoto Nakanishi*[d], *Shigehiro Osada*[a], *Masayoshi Imagawa*[a,*]

[a]*Department of Molecular Biology, Graduate School of Pharmaceutical Sciences, Nagoya City University, 3-1 Tanabe-dori, Mizuho-ku, Nagoya, Aichi 467-8603, Japan*

[b]*Genome Information Research Center, Osaka University, Yamadaoka 3-1, Suita, Osaka 565-0871, Japan*

[c]*Department of Applied Biological Chemistry, Graduate School of Agricultural and Life Sciences, The University of Tokyo, Tokyo 113-8657, Japan*

[d]*Department Cell Biology and Biochemistry, Graduate School of Medical Sciences, Nagoya City University, 1 Kawasumi, Mizuho-cho, Mizuho-ku, Nagoya, Aichi 467-8601, Japan*

ARTICLE INFORMATION

Article Chronology:
Received 17 July 2008
Revised version received
9 November 2008
Accepted 12 December 2008
Available online 29 December 2008

Keywords:
fad104
Adipocyte differentiation
Cell proliferation
Cell adhesion
Cell spreading
Cell migration

ABSTRACT

The molecular mechanisms at the beginning of adipogenesis remain unknown. Previously, we identified a novel gene, *fad104* (factor for adipocyte differentiation 104), transiently expressed at the early stage of adipocyte differentiation. Since the knockdown of the expression of *fad104* dramatically repressed adipogenesis, it is clear that *fad104* plays important roles in adipocyte differentiation. However, the physiological roles of *fad104* are still unknown. In this study, we generated *fad104*-deficient mice by gene targeting. Although the mice were born in the expected Mendelian ratios, all died within 1 day of birth, suggesting *fad104* to be crucial for survival after birth. Furthermore, analyses of mouse embryonic fibroblasts (MEFs) prepared from *fad104*-deficient mice provided new insights into the functions of *fad104*. Disruption of *fad104* inhibited adipocyte differentiation and cell proliferation. In addition, cell adhesion and wound healing assays using *fad104*-deficient MEFs revealed that loss of *fad104* expression caused a reduction in stress fiber formation, and notably delayed cell adhesion, spreading and migration. These results indicate that *fad104* is essential for the survival of newborns just after birth and important for cell proliferation, adhesion, spreading and migration.

* *Corresponding author.* Fax: +81 52 836 3455.
E-mail address: imagawa@phar.nagoya-cu.ac.jp (M. Imagawa).

Abbreviations: fad104, factor for adipocyte differentiation 104; BAT, brown adipose tissue; C/EBP, CCAAT/enhancer binding protein; Dex, dexamethasone; ER, endoplasmic reticulum; FBS, fetal bovine serum; FITC, fluorescein isothiocyanate; FNDC3a, fibronectin type III domain containing 3a; GFP, green fluorescent protein; H&E, hematoxylin and eosin; IBMX, 3-isobutyl-1-methylxantine; Ins, insulin; LC3, microtubule-associated protein light chain; MEFs, mouse embryonic fibroblasts; PBS, phosphate-buffered saline; PCR, polymerase chain reaction; PPARγ, peroxisome proliferator-activated receptor γ; RACE, rapid amplification of cDNA ends; RGS2, regulators of G protein signaling 2; SREBP-1, sterol regulatory element-binding protein 1; sys, symplastic spermatids; TCL/TC10βL, TC10 like/TC10βLong; TRITC, tetramethylrhodamine isothiocyanate; TUNEL, TdT-mediated dUTP-biotin nick end labeling; WAT, white adipose tissue

0014-4827/$ – see front matter © 2008 Elsevier Inc. All rights reserved.
doi:10.1016/j.yexcr.2008.12.013

Introduction

Obesity is a risk factor for many diseases, such as diabetes, hypertension, hyperlipoidemia, and also arteriosclerosis [1]. Obesity is the result of an expansion of individual adipocytes and increase in the overall number of adipocytes. Therefore, to clarify the mechanism of obesity, it is necessary to elucidate the molecular mechanisms by which adipocytes differentiate. It is well established that peroxisome proliferator-activated receptor γ (PPAR γ), the CCAAT/enhancer-binding protein (C/EBP) family, and sterol regulatory element-binding protein 1 (SREBP-1) have crucial roles in the middle and the late stages of the differentiation process [2,3]. However, the events early on in adipogenesis are not fully understood.

Previously, we isolated 102 genes as inducible during the earliest stage of adipocyte differentiation with a polymerase chain reaction (PCR)-subtraction protocol [4,5]. We have identified regulators of G protein signaling 2 (RGS2), TC10-like/TC10βLong (TCL/TC10βL) and p68 RNA helicase as factors accelerating the differentiation process [6–8]. In addition, it was of interest that almost half of the isolated genes were unknown, not being present in the databases. Using the rapid amplification of cDNA ends (RACE) technique and cDNA library screening, we identified four novel genes, factor for adipocyte differentiation 24 (*fad24*), *fad123*, *fad158* and *fad104* [9–12]. Furthermore, we reported that *fad24*, *fad158* and *fad104* were positive regulators of adipocyte differentiation [9,11–13].

FAD104 is a novel protein containing 9 repeats of the fibronectin type III domain and a transmembrane domain. The expression of *fad104* was quickly and transiently elevated at the early stage of adipogenesis and was restricted to the differentiable state. Moreover, the knockdown of *fad104* by RNA interference caused inhibition of the differentiation of 3T3-L1 preadipocytes [12]. These results indicated *fad104* to have an important role in the differentiation.

The fibronectin type III domain contained in FAD104 is found in cell surface receptors and proteins regulating cell adhesion such as fibronectin and vitronectin [14,15]. Fibronectin is one of the extracellular matrix proteins and consists of three types of repeating module, called type I, type II and type III repeats. Fibronectin binds to a variety of extracellular and cell surface molecules, including integrins α5β1 and α4β1 and the HSPG coreceptor syndecan 4, and regulates cell adhesion, spreading, migration, growth and differentiation [16,17]. The Arg-Gly-Asp (RGD) tripeptide sequence in the type III_{10} module of fibronectin plays an important role in the binding of the integrin receptor and activating of integrin-mediated intracellular signals [18,19]. It is of interest that *fad104* also has a RGD tripeptide sequence in the eighth fibronectin type III domain.

In addition, some previous reports indicate that the extracellular matrix proteins including fibronectin and integrins have important roles in adipogenesis [20,21]. The expression of fibronectin and integrin is downregulated during adipogenesis [20]. Furthermore, it was reported that the disruption of contacts with the extracellular matrix was required for adipocyte differentiation [21]. These reports indicate the importance of interaction between the differentiating cells and extracellular matrix, suggesting that the proteins containing the fibronectin type III domain have some crucial role in the differentiation process. However, the role of *fad104* in adipocyte conversion and various cellular functions including cell proliferation, adhesion, spreading and migration is unclear.

In this study, to gain insight into the physiological role of *fad104 in vivo*, we generated mice lacking *fad104*. Although born in the expected Mendelian ratios, the *fad104*-deficient mice all died within 1 day after birth. Interestingly although FAD104 possesses 9 repeats of the fibronectin type III domain, FAD104 localized to the endoplasmic reticulum (ER). Furthermore, analyses of mouse embryonic fibroblasts (MEFs) prepared from *fad104*-deficient mice revealed that disruption of *fad104* caused a reduction in the ability to differentiate, proliferate, adhere, spread and migrate. These results indicate that the novel gene *fad104* is essential for the survival of neonates and promotes not only adipocyte differentiation, but also cell proliferation, adhesion, spreading and migration.

Materials and methods

Generation of the fad104 knockout mouse

The targeting vector was constructed by ligating a 1.0 kb *Xho* I fragment and a 4.4 kb *Xho* I-*Sal* I fragment, which were located upstream and downstream of exon 2, respectively, to the pgk-neo cassette of pLNTK. Both the *Xho* I and *Xho* I-*Sal* I fragments were amplified by PCR using genomic DNA prepared at E14 as a template. The pgk-tk expression cassette was placed next to the short arm for negative selection against random integration. The targeting construct was linearized with the *Sal* I site and electroporated into D3 ES cells. Three positive ES cell clones, screened by Southern blot analyses, were microinjected into C57BL/6 Cr blastocysts purchased from Japan SLC (Shizuoka, Japan). The blastocysts were transferred to ICR pseudopregnant females, resulting in the birth of three lines of male chimeric mice. These male chimeric offspring were mated with C57BL/6 females and chimeras from two lines exhibited germ-line transmission. The F1 agouti offspring mice were then analyzed by Southern blotting and PCR analyses. Heterozygote male mice were backcrossed onto the C57BL/6 background for more than seven generations. All experiments were carried out according to the Guideline for the Care and Use of Laboratory Animals of Nagoya City University Medical School.

Genotyping

For Southern blot analyses, genomic DNA from ES cells and tail snippets was digested with *Bam*HI-*Bgl*II, fractionated on a 1% agarose gel, and blotted onto a Hybond N+ nylon membrane (Amersham Biosciences). Homologous recombination was determined by using as a probe, 500 bp fragments located outside the targeting vector. The filter was hybridized with a probe labeled with [α-^{32}P]-dCTP using a random labeling kit (Takara Biomedicals). The wild-type allele produces a DNA sequence of 5. 4 kb, while the targeted DNA is 2. 0 kb long (Fig. 1A).

Measurements of body temperature, blood glucose level and brown adipose tissue (BAT) weight

Newborn pups were obtained by caesarean delivery at E18.5. Just after caesarean section, a thermistor (PHYSITEMP INSTRUMENTS INC.) was introduced into the rectum of pups for body temperature measurements. BAT was isolated from the interscapular space of newborn pups, and measured its weight. Blood

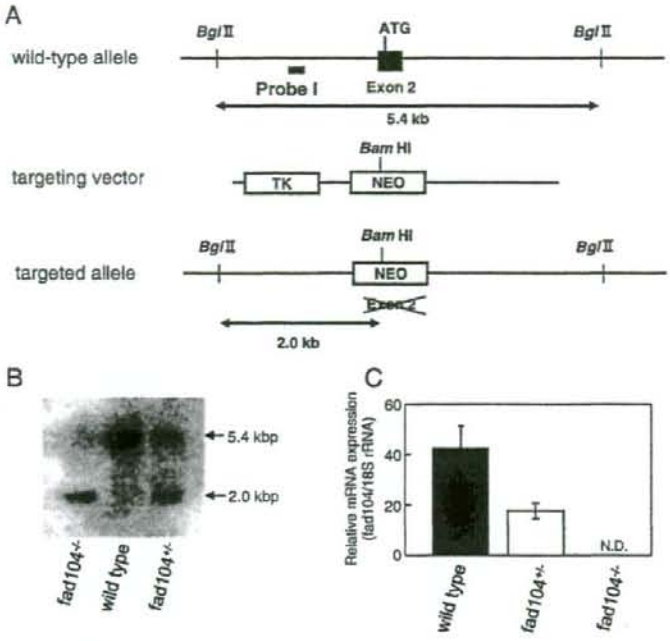

Fig. 1 – Targeted disruption of the *fad104* gene. (A) Schematic representation of the wild-type and targeted alleles. The black box represents exon 2 of the *fad104* gene. The white boxes represent pgk-neo and pgk-tk cassettes. The probe used for Southern blot analysis is shown as Probe I. (B) Southern blot analysis of mouse genomic DNA. The expected DNA fragments for the targeted allele and the wild-type allele are 2.0 and 5.4 kb, respectively. (C) Q-PCR analysis of mRNA from embryonic fibroblasts isolated from each of the genotypes. The expression level of *fad104* was normalized with 18S rRNA expression determined by Q-PCR. The data represent means with standard deviations ($n=3$).

glucose level was measured by the Glucose CII-Test (Wako Pure Chemical).

Preparation of MEFs and adipocyte differentiation

MEFs were isolated from decapitated embryonic day 13.5 embryos of wild type and *fad104*$^{-/-}$ mice. According to the previous reports, MEFs were used at low passage numbers (2 to 4 times) throughout the studies to avoid accumulative genetic abnormalities during passage [22,23]. Cells were cultured in α-modified Eagle's medium (α-MEM; Invitrogen) supplemented with 10% fetal bovine serum (FBS).

Induction of adipogenic differentiation was carried out according to methods described previously [24]. Briefly, MEFs (2 times passage) were seeded in culture dishes. The medium was changed to α-MEM supplemented with 0.5 mM 3-isobutyl-1-methylxantine (IBMX), 5 μg/ml of insulin (Ins), 1 μM dexamethasone (Dex), and 10% FBS at 2 days postconfluence. This medium was renewed every other day. The amounts of triacylglycerol were measured using LIPIDOS LIQUID (Ono) according to the manufacturer's instructions.

Implantation and histological analyses

MEFs (4 times passage) were grown to near confluence and trypsinized. After centrifugation, cell pellets were suspended in α-MEM containing 10% FBS and injected subcutaneously (3×10^7 cells per site) with a 21-gauge needle at the back of BALB/c athymic mice (Charles River Laboratories). Three weeks after implantation, these mice were killed by cervical dislocation, and the fat pads derived from the implanted cells were excited and fixed in 10% formalin in phosphate-buffered saline (PBS). The specimens were cut into 4-μm-thick sections and stained with hematoxylin and eosin (H&E). For lipid staining with osmium tetroxide (OsO_4), the retrieved implants were fixed in 2.5% glutaraldehyde in PBS for 15 min and 10% formalin in PBS. To cross-link intracellular lipids, the implants were covered with a 1% OsO_4 solution for 2 h on ice. After excess OsO_4 was removed by washing with distilled water, the implants were fixed again with 10% formalin in PBS, and embedded in paraffin. The specimens were cut into 6-μm-thick sections and deparaffinized to observe OsO_4-stained lipids.

Real-time quantitative RT-PCR (Q-PCR)

Total RNA was extracted using TRIzol (Invitrogen). For Q-PCR, cDNA was prepared using ReverTra Ace-α- (TOYOBO) following the manufacturer's recommended procedures. An ABI PRISM 7000 sequence detection system (Applied Biosystems) was used to perform Q-PCR. The pre-designed primers and probe sets of *fad104* and 18S rRNA were obtained from Applied Biosystems. The reaction mixture was prepared using a TaqMan Universal PCR

Master Mix (Applied Biosystems) according to the manufacturer's instructions. The mixture was incubated at 50 °C for 2 min and at 95 °C for 10 min, and then the PCR was done at 95 °C for 15 s and at 60 °C for 1 min for 40 cycles. The relative standard curves were generated in each experiment to calculate the input amounts of the unknown samples.

Subcellular localization of FAD104

An amino terminal Flag tagged FAD104 expression plasmid, pFlag-fad104, and a carboxy terminal green-fluorescent protein (GFP) tagged FAD104 expression plasmid, pfad104-GFP, were constructed by subcloning the coding region of *fad104* into p3xFlag-CMV7.1 (SIGMA) and pEGFP-N1 (BD Biosciences), respectively.

NIH-3T3 cells were plated onto cell disks (SUMITOMO BAKELITE Co., Ltd) 1 day before transfection. The cells were transfected using the calcium co-precipitation method, fixed with 2% paraformaldehyde in PBS and permeabilized with 0.2% Triton X-100. Each cell disk was incubated with primary antibody, rabbit polyclonal anti-calnexin antibody (H-70) (Santa Cruz Biotechnology) and mouse monoclonal anti-Flag antibody (SIGMA), for 1 h at room temperature. After 5 washes with PBS, tetramethylrhodamine isothiocyanate (TRITC)-conjugated anti-rabbit and fluorescein isothiocyanate (FITC)-conjugated anti-mouse antibodies were reached for 1 h at room temperature. After 5 washes with PBS, the signals for GFP, FITC and TRITC were detected by confocal laser scanning microscopy (LSM510META, Carl Zeiss Co., Ltd).

Cell proliferation and cell death assay

Two times passage MEFs were used in this study. The cells (3×10^4) were seeded into 6-well tissue culture plates and trypsinized. Numbers of cells were counted at various time points during the cell growth period. For the detection of cell death, TdT-mediated dUTP-biotin nick end labeling (TUNEL) assays were performed using the In Situ Cell Death Detection kit, Fluorescein (Roche) according to the manufacturer's instructions.

Cell adhesion assay

Four times passage MEFs were used in this study. The cells (1×10^4) were plated onto fibronectin-coated (3 μg/ml) 24-well plates. For the coating of fibronectin, human fibronectin (SIGMA) was incubated for 1 h at room temperature. At specific time points, the unattached cells were washed away with PBS. The attached cells were fixed for 10 min in 2% paraformaldehyde in PBS at room temperature. After 3 washes with PBS, the attached cells were photographed, and counted in five random microscopic fields per plate.

Immunofluorescence microscopy

Four times passage MEFs were used in this study. MEFs (4×10^4) were replated on fibronectin-coated (3 μg/ml) cell disks in 24-well plates. At different time points, cell disks were fixed for 10 min in 2% paraformaldehyde in PBS and permeabilized with 0.2% Triton X-100. The cell disks were incubated with anti-vinculin monoclonal antibody (SIGMA) for 1 h at room temperature. After 3 washes with PBS, FITC-conjugated anti-mouse secondary antibody and TRITC-conjugated phalloidin (Jackson ImmunoResearch) for detection of the F-actin structure of the cells were reacted for 1 h at room temperature. After 3 more washes with PBS, FITC and TRITC signals were detected by fluorescence microscopy (BX51, OLYMPUS).

Wound healing assay

Four times passage MEFs were used in this study. MEFs of wild-type and *fad104*$^{-/-}$ mice were grown to confluence in 60 mm dishes. At 1 day postconfluence, four sites in each plate were scraped with a yellow plastic pipette tip to generate scratch wounds. The medium was removed and replaced with fresh medium. The cells were incubated at 37 °C for 10 h. The wound areas at various points were photographed and measured using NIH-Image J software.

Statistical analyses

Data are expressed as the mean±standard deviation (S.D.) or the mean±standard error (S.E.). All data presented with statistical analyses were analyzed using a Student's *t* test. *p* values less than 0.05 were considered to be significant.

Results

Disruption of the fad104 gene causes rapid postnatal death

To explore the function of *fad104 in vivo*, we generated *fad104*-deficient mice. We previously indicated that the mouse *fad104* was located at chromosome 3 and constituted 26 exons [12]. To disrupt the *fad104* gene, the targeting vector was designed to remove the second exon of *fad104*, which included the translational start site (Fig. 1A). The targeting vector was introduced into D3 ES cells and positive cells were selected using G418 and ganciclovir. Three of the targeted ES cell lines were injected into C57BL/6 Cr blastocysts, and chimeric male mice were obtained. Of these, two lines of mice exhibited germ-line transmission. Intercrosses of the heterozygote mice were used to establish the homozygote *fad104*-deficient mice.

First, we analyzed the genotype of mice in the heterozygote intercross at 4 weeks of age. However, *fad104*$^{-/-}$ mice were not found among 55 live-born progenies. Then, we observed the fate of the newborn mice at 1 day of birth. As shown in Table 1, ten of 47 pups obtained from crosses between heterozygote mice had already died, and three more pups died the next day. Southern blot analysis indicated that 13 newborns that died within 1 day of birth were homozygous mutants, which is almost equal to the expected Mendelian ratio (Table 1, Fig. 1B). Furthermore, Q-PCR analysis using MEFs prepared from offspring of the heterozygote intercross confirmed that *fad104*-deficient mice do not express *fad104* (Fig. 1C).

Table 1 – Genotype of progeny of heterozygote intercrosses

Age	No. of mice with genotype		
	+/+	+/−	−/−
E 18.5	9	24	13
P1	13	21	13[a]
4-week	19	36	0

[a] Ten newborns had died. Another 3 newborns died within 1 day.

To determine whether disruption of *fad104* causes lethality during embryogenesis, we next examined the genotype of newborns from the heterozygote intercross at E18.5. Just minutes after caesarean section, all pups at E18.5 were alive, and exhibited the expected Mendelian ratio (Table 1). However, all the *fad104*$^{-/-}$ offspring died within 15 min after caesarean section, whereas the wild-type and *fad104*$^{+/-}$ neonates survived. Similar results were observed for other *fad104*-deficient mice, which were obtained from independent ES clones. These results strongly suggest that the disruption of *fad104* causes rapid postnatal death.

To clarify the causes of rapid postnatal death by the disruption of *fad104*, we examined whether *fad104* is involved in the energy homeostasis just after birth (Fig. 2). We first measured the body weights and blood glucose levels of *fad104*$^{-/-}$ neonates. The body weights and blood glucose levels of *fad104*$^{-/-}$ neonates were not significantly different from those of wild-type and *fad104*$^{+/-}$ pups (Figs. 2A and B). Just after birth, the thermoregulation is very important to maintain energy homeostasis. Therefore, we next measured the body temperatures of newborn pups just after caesarean. The body temperatures did not differ among three genotypes (Fig. 2C). Furthermore, we measured weights of BAT isolated from the interscapular space of neonates. The weights of BAT of *fad104*$^{-/-}$ neonates were not also different from those of wild-type and *fad104*$^{+/-}$ pups (Fig. 2D). These results may indicate that the rapid postnatal death observed in *fad104*-deficient infants is not caused by the failure of energy homeostasis.

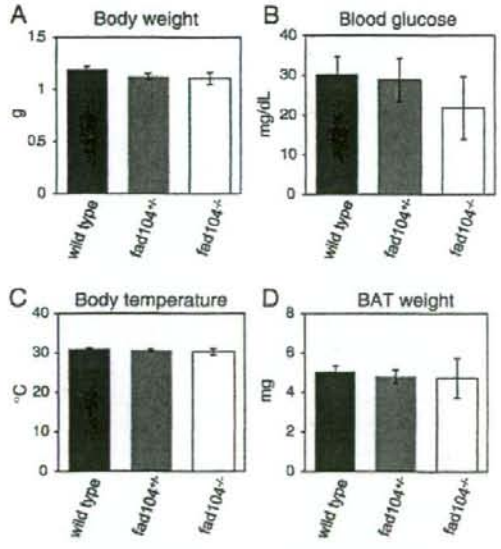

Fig. 2 – Characterization of *fad104*-deficient mice at embryonic day 18.5. Body weights, blood glucose levels, body temperatures and BAT weights of neonates were measured just after caesarean section. (A) Body weights (wild-type, $n=17$, *fad104*$^{+/-}$, $n=36$, *fad104*$^{-/-}$, $n=9$). (B) Body temperatures (wild-type, $n=10$, *fad104*$^{+/-}$, $n=11$, *fad104*$^{-/-}$, $n=4$). (C) Blood glucose levels (wild-type, $n=12$, *fad104*$^{+/-}$, $n=14$, *fad104*$^{-/-}$, $n=5$). (D) BAT weights (wild-type, $n=10$, *fad104*$^{+/-}$, $n=11$, *fad104*$^{-/-}$, $n=4$). Each column represents the mean with standard error.

Fad104-deficient MEFs exhibit reduced adipogenesis

Since the disruption of *fad104* causes postnatal death, it is clear that *fad104* has an important role in the survival of newborn. Our previous report indicated that *fad104* promoted the differentiation of 3T3-L1 preadipocytes [12]. Therefore, using the MEFs prepared from *fad104*-deficient mice, we first examined the role of *fad104* in the conversion to adipocytes.

We investigated the expression of *fad104* during the differentiation of MEFs prepared from wild-type embryos. The level of *fad104* quickly elevated after the induction, and reached a peak at 3 h as found in 3T3-L1 cells (Fig. 3A). Next, we performed a differentiation experiment. Wild-type and *fad104*$^{-/-}$ MEFs were brought to confluence in 10% FBS. After 2 days of incubation, the medium was changed to the differentiated medium. After 12 days, the cells were stained with Oil Red O to detect oil droplets (Fig. 3B) and the amounts of triacylglycerol were determined (Fig. 3C). Under these conditions, approximately 50% of MEFs from wild-type embryos could differentiate into adipocytes. On the other hand, little accumulation of oil droplets and triacylglycerol in MEFs from *fad104*$^{-/-}$ embryos was observed.

Next, MEFs prepared from wild-type and *fad104*$^{-/-}$ embryos were implanted subcutaneously into the back of athymic mice. After 3 weeks, the implants were excited. The weights of the implants derived from *fad104*$^{-/-}$ MEFs were indistinguishable from those of wild-type MEFs (data not shown). In order to observe the histological characterization of implants, the cells accumulated oil droplets were detected by H&E and OsO_4 staining. The implanted wild-type MEFs developed into adipocytes and stored oil droplets. In contrast, the implanted *fad104*$^{-/-}$ MEFs failed to develop into mature adipocytes (Fig. 4). These results combined with our previous observations demonstrated that *fad104* has an important role for the differentiation of MEFs as well as of mouse 3T3-L1 cells.

FAD104 localized to the endoplasmic reticulum (ER)

To determine the subcellular localization of FAD104, Flag-fad104 chimeric plasmid was transiently introduced into NIH-3T3 cells and the signals were detected by confocal scanning laser microscopy. The signals of Flag-FAD104 were observed in the cytoplasm (Fig. 5A). Because FAD104 possesses a transmembrane domain at the C-terminus, it seems that FAD104 distributes to the membrane structure in the cytoplasm. Therefore, we further conducted immunofluorescent staining using antibody against calnexin, which is a marker for the ER. The distribution of Flag-FAD104 overlapped with the staining pattern of calnexin (Fig. 5A). Since Flag-fad104 chimeric construct have Flag tag at the N-terminal site, we further constructed fad104-GFP chimeric plasmid in which GFP stays in the C terminus and introduced into NIH-3T3 cells. As shown in Fig. 5B, FAD-GFP was also distributed in the cytosol and overlapped with calnexin. These results demonstrated that the type and position of tags do not affect the distribution and FAD104 localized to the ER.

Cell proliferation was inhibited in fad104-deficient MEFs

The experiments of subcellular localization of FAD104 demonstrated that FAD104 is a novel ER protein. However, it is unclear whether *fad104* is involved in cellular functions including cell proliferation, cell adhesion, cell spreading and cell migration. To elucidate the function of *fad104*, we further analyzed *fad104*-deficient MEFs.

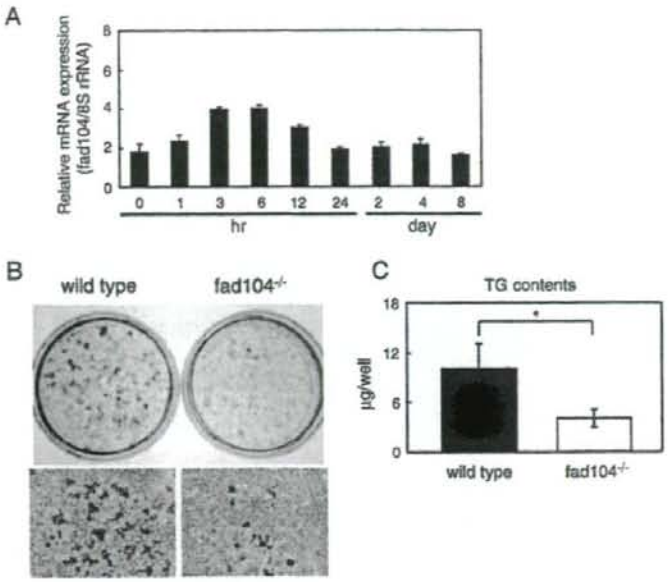

Fig. 3 – Adipocyte differentiation of MEFs from wild-type and homozygous *fad104*-deficient embryos. (A) Q-PCR analyses of *fad104* expression in MEFs from wild-type embryos. The expression level of *fad104* was determined at various time points in the differentiation of MEFs from wild-type embryos and normalized with 18S rRNA expression determined by Q-PCR. The data represent means with standard deviations ($n=3$). (B) Differentiation of MEFs from wild-type and *fad104*$^{-/-}$ embryos. Wild-type and *fad104*$^{-/-}$ MEFs were treated with the differentiation medium containing IBMX, Dex, Ins and FBS. These cells after 12 days treatment were stained with Oil Red O. Oil Red O staining of plates (upper) and microscopic examination (lower). (C) The amounts of triacylglycerol. The measurement of triacylglycerol content was done on 24-well plates. Each column represents the mean with standard deviations ($n=3$). *$p<0.05$.

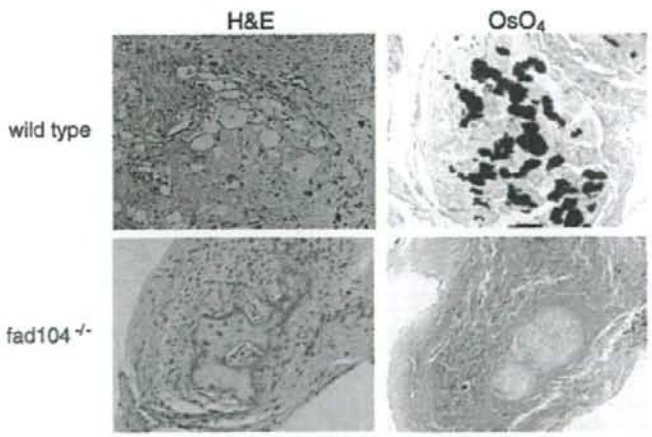

Fig. 4 – Histological analyses of the implanted MEFs from wild-type and fad104-deficient embryo. At 3 weeks after implantation of MEFs prepared from wild-type (upper panels) and *fad104*$^{-/-}$ (lower panels) embryos, the implants were excited and stained by H&E (left panels) and OsO_4 (right panels).

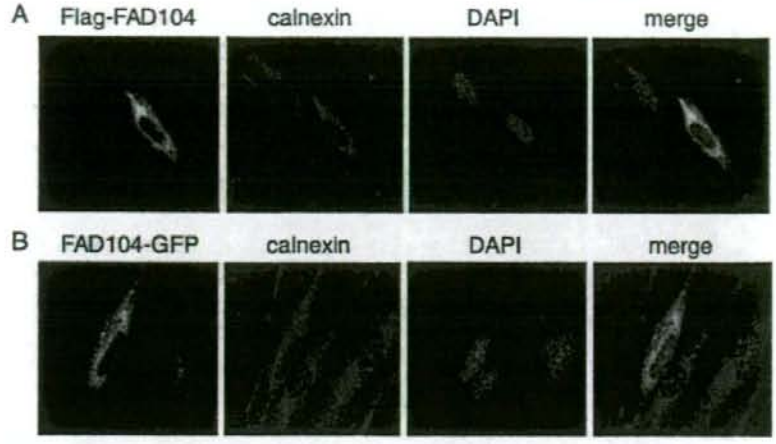

Fig. 5 – Subcellular localization of FAD104. (A) Subcellular localization of Flag-FAD104. NIH-3T3 cells were transiently transfected with Flag-*fad104*-expression plasmid. After conducting immunofluorescent staining using anti-Flag and anti-calnexin, the signals of Flag-FAD104 (green) and calnexin (red) were detected with confocal laser scanning microscopy. (B) Subcellular localization of FAD104-GFP. NIH-3T3 cells were transiently transfected with *fad104*-GFP-expression plasmid. Transfected NIH-3T3 cells were fixed and performed the immunofluorescence analyses staining with anti calnexin. Fluorescence of FAD104-GFP (green) and calnexin (red) were detected with confocal laser scanning microscopy.

First, we investigated the rate of cell proliferation of wild-type and *fad104*$^{-/-}$ MEFs. MEFs prepared from wild-type and *fad104*$^{-/-}$ embryos were seeded in tissue cultures, and counted at various time points. As shown in Fig. 6, the *fad104*-deficient MEFs exhibited a slightly decrease in proliferation compared with the wild-type MEFs. To exclude the possibility that the decrease of proliferating rate by the disruption of *fad104* was caused by the increase the cell death including anoixis, we performed TUNEL assay to detect cell death during proliferation in MEFs prepared from wild-type and *fad104*$^{-/-}$ embryos. At 2, 4, and 6 days after seeding, no TUNEL-positive cells were observed in wild-type and *fad104*$^{-/-}$ MEFs (data not shown). The difference of cell proliferation between wild-type and *fad104*$^{-/-}$ MEFs may not be caused by cell death. These results indicated that the disruption of *fad104* inhibits cell proliferation.

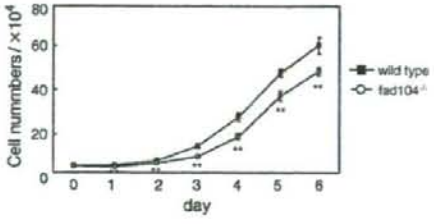

Fig. 6 – Cell proliferation was inhibited in *fad104*-deficient MEFs. MEFs from wild-type and *fad104*$^{-/-}$ embryos were seeded in 6-well tissue culture plates at a total 3×10^4 cells/well. These cells were trypsinized and counted. The data represent means with standard deviations ($n=4$) $^{**}p<0.01$.

Deficiency of fad104 reduced stress fiber formation and caused a delay in cell adhesion and cell spreading

Next, to examine the effect of disruption of *fad104* on cell adhesion, cell spreading and the actin cytoskeleton's organization, we stained F-actin of wild-type and *fad104*$^{-/-}$ MEFs with TRITC-conjugated phalloidin. In addition, to detect the focal complex in wild-type and *fad104*$^{-/-}$ MEFs, the localization of vinculin was visualized using anti-vinculin antibody.

At 30 min from seeding, the wild-type MEFs already showed cell spreading and the formation of long actin stress fibers. In contrast, the *fad104*$^{-/-}$ MEFs were significantly delayed in spreading, and caused a lack of actin stress fibers and the appearance of F-actin rich membrane ruffles (Fig. 7A). At 120 min, in wild-type MEFs, the actin stress fibers were notably increased and co-localized with vinculin at the end of these fibers at focal adhesion sites. Furthermore, the morphology also changed to that of fibroblasts. In contrast, few stress fibers and morphological changes were observed in *fad104*$^{-/-}$ MEFs. In addition, vinculin in *fad104*$^{-/-}$ MEFs was not distributed to focal adhesion sites, and not co-localized with actin stress fibers (Fig. 7A). After 480 min, *fad104*$^{-/-}$ MEFs had spread more than was observed at 120 min, and developed actin stress fibers with vinculin at their ends, but were still less well spread than wild-type MEFs (Fig. 7A). These results indicated that the disruption of *fad104* reduced the numbers of stress fibers formed and cell adhesion sites, and delayed the change in cell morphology and cell spreading.

To test whether *fad104* regulates cell adhesion, we further performed a quantitative cell adhesion assay by counting the attached cells in the tissue culture. Wild-type and *fad104*$^{-/-}$ MEFs were plated onto fibronectin-coated plates. The attached cells